UNIVERSITY OF AMSTERDAM

UvA-DARE (Digital Academic Repository)

Fluorescent Labeling to Investigate Nanopatterning Processes in Extreme Ultraviolet Lithography

Wu, L.; Hilbers, M.F.; Lugier, O.; Thakur, N.; Vockenhuber, M.; Ekinci, Y.; Brouwer, A.M.; Castellanos, S.

DOI
10.1021/acsami.1c16257

Publication date
2021

Document Version
Final published version

Published in
ACS Applied Materials and Interfaces

License
CC BY-NC-ND

Link to publication

Citation for published version (APA):
Wu, L., Hilbers, M. F., Lugier, O., Thakur, N., Vockenhuber, M., Ekinci, Y., Brouwer, A. M., & Castellanos, S. (2021). Fluorescent Labeling to Investigate Nanopatterning Processes in Extreme Ultraviolet Lithography. *ACS Applied Materials and Interfaces*, *13*(43), 51790-51798. https://doi.org/10.1021/acsami.1c16257

General rights
It is not permitted to download or to forward/distribute the text or part of it without the consent of the author(s) and/or copyright holder(s), other than for strictly personal, individual use, unless the work is under an open content license (like Creative Commons).

Disclaimer/Complaints regulations
If you believe that digital publication of certain material infringes any of your rights or (privacy) interests, please let the Library know, stating your reasons. In case of a legitimate complaint, the Library will make the material inaccessible and/or remove it from the website. Please Ask the Library: https://uba.uva.nl/en/contact, or a letter to: Library of the University of Amsterdam, Secretariat, P.O. Box 19185, 1000 GD Amsterdam, The Netherlands. You will be contacted as soon as possible.
UvA-DARE is a service provided by the library of the University of Amsterdam (https://dare.uva.nl)

Download date:10 Sep 2026

ACS APPLIED MATERIALS & INTERFACES

www.acsami.org

Research Article

Fluorescent Labeling to Investigate Nanopatterning Processes in Extreme Ultraviolet Lithography

Lianjia Wu,* Michiel F. Hilbers, Olivier Lugier, Neha Thakur, Michaela Vockenhuber, Yasin Ekinci, Albert M. Brouwer, and Sonia Castellanos*

Cite This: *ACS Appl. Mater. Interfaces* 2021, 13, 51790–51798

Read Online

ACCESS | Metrics & More | Article Recommendations | Supporting Information

ABSTRACT: Extreme ultraviolet (EUV) lithography uses 13.5 nm light to reach the sub-20 nm resolution. However, the process of pattern formation induced by this high-energy light is not well-understood. In this work, we provide an inorganic EUV photoresist with fluorescence properties by introducing a carbazole derivative as a ligand, and we study its effect on the patterning process. Using the fluorescence properties, changes in the emission of the material after EUV exposure could be tracked by means of spectroscopy and microscopy. The resist sensitivity was substantially reduced by the incorporation of the carbazole benzoate ligands, which is attributed to hole trapping and steric hindrance. After EUV irradiation of the resist films, infrared, UV–visible absorption, and fluorescence spectroscopies showed that the carbazole units were still mostly intact, although their fluorescence intensity was lowered. Our work shows that fluorescent labeling can provide relevant mechanistic insights in the patterning process of resists, potentially with a molecular resolution.

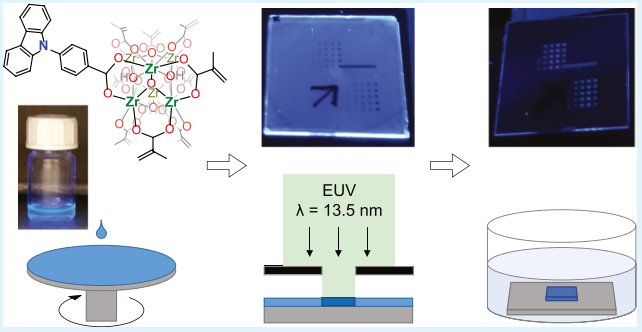

KEYWORDS: *EUV resist, Zr–oxo cluster, fluorescence microscopy, radiation chemistry, carbazole*

Downloaded via UNIV AMSTERDAM on April 28, 2022 at 10:47:31 (UTC).
See https://pubs.acs.org/sharingguidelines for options on how to legitimately share published articles.

INTRODUCTION

Photolithography is a process to manufacture micro-/nanoelectronics in which a mask is used to project light with a desired pattern on a photosensitive layer—known as a (photo)resist—that coats a silicon wafer. After the exposure, either the irradiated or nonirradiated parts of the photoresist can be selectively removed in a solvent called the developer. This is a consequence of the chemical reactions occurring in the irradiated part, which lead to different solubility properties compared to that of the pristine material. The patterned photoresist acts as a sacrificial template that allows the transfer of the desired pattern to the silicon wafer underneath during an etching step. Currently, the fabrication of nanostructures with features smaller than 30 nm using the state-of-the-art deep ultraviolet lithography (DUVL) requires immersion lithography[1] with double or multiple patterning processes to overcome the inherent diffraction limit associated with the employed wavelength (193 nm, E = 6.4 eV).[2−4] In contrast, with the newly developed extreme ultraviolet lithography (EUVL), the desired small features can be printed in one patterning cycle due to its shorter wavelength (13.5 nm, E = 92 eV). Therefore, although DUVL still dominates in semiconductor manufacture, EUVL has been launched into the market for the next generation of chips with even smaller features and higher computing performance. Nevertheless, one of the critical points for EUVL to be established in the market is that new photoresist materials with optimal performance need to be developed.

Ideally, EUV photoresists should be able to print the targeted features using doses of EUV light below 20 mJ/cm^2 in order to make this technique cost-effective. In addition, for the optimal operation of the fabricated circuits, the tolerance for variability in the feature dimensions is very low (<15%). In lithographic terms, materials that have high sensitivity, can print low critical dimensions (resolution), and yield low line edge roughness are desired. Such requirements imply that (1) the very thin films of the resist material (20–30 nm) should have high linear absorptivity values (*ca.* 12–18 μm^{-1}) at 13.5 nm and (2) the quantum yields of the processes that render changes in the material's solubility should be high. However, EUV-induced radiation chemistry in photoresists is not yet as well-understood as the photochemistry triggered by DUV light,[5,6] which hinders the rational design of materials that fulfill the abovementioned desired properties. This is because the chemical reactions induced by EUV photons are the

Received: August 25, 2021
Accepted: October 6, 2021
Published: October 20, 2021

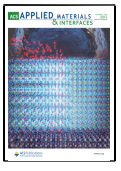

ACS Publications

© 2021 The Authors. Published by American Chemical Society

Scheme 1. Functionalization of ZrMc by Ligand Exchange

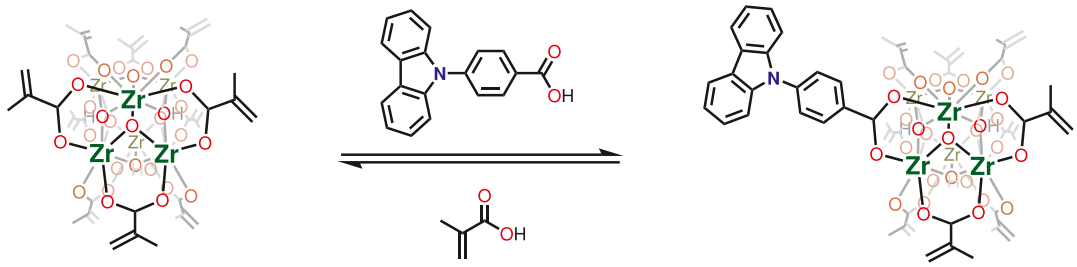

consequence of multiple processes, such as ionization events and the generation of electron cascades in the photoresist.[7]

Metal-containing inorganic−organic hybrid molecular materials, such as metal−oxo clusters (MOCs), are being considered as potential EUV photoresists.[8−11] In their core-/shell-like molecular structure, the metal−oxo core generally contributes the most to the EUV absorptivity and to the etching resistance, while the organic ligand shell determines the reactivity that renders the solubility switch. In MOCs with carboxylate ligands, the dynamic behavior of carboxylates in solution enables us to modify the composition of the ligand shell *via* exchange reactions[12,13] and therefore potentially to combine different functionalities in the resulting material.

A relatively unexplored way to investigate the lithographic process in a photoresist is to use fluorescent labels. For instance, they can be used to image the transfer of the optical projection to the material. Fluorescent dyes have been employed in the research of the polymer-based photoresist used in microlithography.[14−16] However, the blended small molecules of fluorescent labels can aggregate in the polymer matrix and induce defects in the patterned photoresist films.[17,18] This limits the use of these labels for photoresist research, especially as the requirements for nanolithography become more constraining in terms of resolution and line width roughness. As an alternative, fluorescent ligand doping in MOCs can facilitate the dispersion of the fluorescent label and prevent phase separation as in this case, the ligand is chemically bonded and is thus part of the discrete entities that form the molecular material.

Here, we report a methacrylate (Mc) zirconium oxo cluster $Zr_6O_4(OH)_4(OMc)_{12}$ (denoted as **ZrMc**) functionalized with a fluorescent carboxylate ligand, 4-(9*H*-carbazol-9-yl)benzoate (CB). The carbazole unit was incorporated into **ZrMc** *via* a ligand exchange reaction in a ratio of one fluorescent label per molecule, that is, the resulting material, noted as **ZrMc−CB**, features a CB/Mc ratio of 1:11 on average (Scheme 1). This means that the deposited photoresist film retains a high concentration of Mc in the organic ligand shell so that the material's processability and reactivity can be preserved.

The influence of the fluorescent CB ligand can be expected on four aspects of the MOC-based EUV photoresist. First, from an application point of view, the CB ligand incorporated in the precursor MOC can work as a fluorescent label for the detection of the residual resist after the development, for the endpoint of etching,[14] or for the fabrication of fluorescent patterns. Furthermore, fluorescence microscopy could become a new metrology tool for the characterization of photoresist patterning since it is a noninvasive technique, as opposed to scanning electron microscopy (SEM), and can offer molecular resolution by means of super-resolution fluorescence imaging techniques.[19] In fact, the accurate metrology of the ever-decreasing printed features is becoming a major challenge, and the research on optical-based alternative methods to SEM is currently being pursued.[20] Second, extended aromatic structures have lower electronic band gaps, which provide higher valence band energies than the precursor MOC. Therefore, doping with an extended aromatic carboxylate is expected to lower the ionization potential of the MOCs.[21] This could potentially yield more electrons in the secondary electron cascade induced by EUV photons, leading to higher reactivity and sensitivity. On the other hand, this type of ligand also stabilizes the radical cations generated after the ionization,[21] thus preventing the subsequent decarboxylation and cross-linking reactions. The latter two reactions have been demonstrated as the main contributions to the solubility switch mechanism of **ZrMc** as an EUV photoresist[22] and for similar materials.[23,24] Therefore, doping with CB could also lead to a third change in the **ZrMc** properties: the decrease in sensitivity due to the lower reactivity. The fourth aspect to consider is that this extended aromatic carboxylate ligand is bulky, which can increase the average intermolecular distance of **ZrMc** in the solid state. A longer packing distance can lead to lower reactivity because it decreases the probability of intermolecular cross-linking between Mc ligands. In summary, the introduction of the fluorescent ligand could affect the reactivity in a positive or negative way.

In this work, we examined the influence of incorporating a CB ligand in the **ZrMc** MOC on its lithographic performance and used the fluorescence properties provided by this ligand to investigate the structural changes occurring on the **ZrMc−CB** resist after EUV exposure together with complementary Fourier-transform infrared (FTIR) and UV−visible absorption spectroscopies. The spectroscopic results indicate that in the functionalized MOC, the carbazole unit is rather inert, while the Mc ligands are the main contribution to the EUV-induced reactivity of the photoresist material. Nevertheless, the phenylcarbazole unit interferes with the cross-linking mechanism that renders the solubility switch of the material. Our work explores alternative ways of investigating EUV nanopatterning processes and provides an understanding of the role of different organic components/functional groups in the design of new EUV photoresist materials.

EXPERIMENTAL SECTION

Synthesis. Reagents and solvents were purchased from Sigma-Aldrich and dried with molecular sieves before use. $Zr_6O_4(OH)_4(OMc)_{12}$ was synthesized by the reaction of zirconium(IV) propoxide with 4 molar equivalents of methacrylic acid in dry air instead of inert gas, adapted from the method which has been reported.[25] 4-(9*H*-Carbazol-9-yl)benzoic acid (CBA) was synthesized as reported previously.[26,27] The dynamics of ligand exchange in solution was evidenced by the ^1H and ^{13}C NMR spectra of 1:1 (molar

https://doi.org/10.1021/acsami.1c16257
ACS Appl. Mater. Interfaces 2021, 13, 51790−51798

ratio) CBA/ZrMc in CD_2Cl_2 where peak broadening and changes in the chemical shift were observed (Figure S1).

Thin-Film Deposition. To a solution (0.9 mL) of CBA (5.1 mg, 17.7 mmol) in chloroform (3.0 mL), **ZrMc** (9.0 mg, 5.3 mmol) was added. The resulting reaction mixture was sonicated for 2 min, and then, 0.1 mL of propylene glycol methyl ether acetate was added. The solution was sonicated for another 2 min and filtered before spin-coating. Thin films were spin-coated at a spinning rate of 2100 rpm for 30 s with an acceleration of 3000 rpm/s onto Si substrates for patterning tests and for FTIR spectroscopy and on quartz substrates for UV−visible absorption and fluorescence spectroscopies. The samples were baked at 90 °C for 30 s after spin-coating to remove the residual solvents. The reference **ZrMc** thin film was prepared in the same way without adding CBA. All the thin films were prepared in ambient conditions.

EUV Exposure and Characterization. The spin-coated thin films were irradiated with EUV light at the XIL-II beamline of the Swiss Light Source in the Paul Scherrer Institute. Samples for dense line−space patterning were exposed using the EUV interference lithography tool with periodic line/space patterns of pitches of 44, 60, 80, and 100 nm. Samples were exposed with an open-frame mask of 0.5 × 0.5 mm^2 aperture at varied doses from 2 and 4 to 994 mJ/cm^2 for contrast curve and fluorescence intensity measurements, respectively. Samples for fluorescence, infrared, and UV−visible absorption spectroscopies were exposed with a 1.7 × 1.7 mm^2 aperture. The exposure areas were adjacent in a 4 × 4 square matrix at a single dose of 85, 170, or 425 mJ/cm^2 in order to attain a large exposed area to record the full spectra in the spectrometer (no spatial resolution). These four doses were chosen as they cover the different regimes in the contrast curve and therefore track the decrease in the solubility of the resist in the developer: from the middle of the contrast curve slope, through a dose at which the whole thickness turns insoluble, to a dose that overexposes the resist. In the chosen illumination conditions, the beam power is 14.9 mW/cm^2 (around 2 ns pulse period and 30 ps pulse width). After the exposure, the sample was immersed in chloroform for 30 s without further processing for all developed samples.

Fluorescence spectra were measured with a HORIBA SPEX Fluorolog 3 spectrometer. The sample was fixed vertically in the measurement chamber with the resist film facing the excitation beam perpendicular and emission detected on the side. The emission spectra were obtained with the excitation at 345 nm with a bandwidth of 3 nm, recorded from 360 to 630 nm with a bandwidth of 3 nm and averaged with three measurements. UV absorption spectra of **ZrMc** and **ZrMc−CB** were obtained with a Shimadzu UV-2600 spectrophotometer. FTIR spectra of thin films were recorded on a Bruker VERTEX 80v vacuum FTIR spectrometer, and fast-Fourier transform (FFT) low-pass filtering was applied to the spectra with the cutoff frequency of 0.04 Hz to remove the interference fringes in the high-wavenumber range. The thickness of the samples was measured at the edge of the developed samples or using a scratch made on the spin-coated thin film on a Bruker atomic force microscope (Dimension Icon) with the ScanAsyst mode. The top−down SEM image of the line−space pattern was recorded using a FEI Verios 460 scanning electron microscope with a high voltage of 5.0 kV.

Fluorescence Intensity and Lifetime Measurements. The fluorescence emission intensity of **ZrMc−CB** exposed at each applied dose of EUV was recorded in the middle of each exposed field using a PicoQuant MicroTime 200 confocal microscope coupled with a frequency-doubled tunable Ti:sapphire laser (Chameleon Ultra, Coherent; λ_{exc} = 345 nm—by frequency doubling the 690 nm fundamental—and a dichroic filter cutoff at 400 nm). The emission was selected with a 447/60 band-pass filter and detected with a single-photon avalanche photodiode (SPCM CD2801 from PerkinElmer). Simultaneously with the intensity, time-correlated single-photon counting data were obtained with a TimeHarp 200 photon-counting unit. The width of the instrument response function (IRF) was ∼0.25 ns. The decay curves were fitted to the convolution of a Gaussian IRF with the biexponential decay $I(t) = A_1 \exp(-t/\tau_1) + A_2 \exp(-t/\tau_2)$ using Igor Pro version 7 (WaveMetrics). The average lifetimes reported are $\tau_{av} = (A_1\tau_1^2 + A_2\tau_2^2)/(A_1\tau_1 + A_2\tau_2)$. The fluorescence intensity at each dose was quantified from the recorded image (field of view: 80 × 80 μm^2 and resolution: 2.5 pixels per μm) using ImageJ (version 1.52h) software.

Theoretical Calculations. Density functional theory calculations were performed using the Gaussian 16 package[28] with the B3LYP hybrid density functional and the Def2SVP[29,30] basis set.

RESULTS AND DISCUSSION

EUV Lithography. To evaluate the lithographic performance of **ZrMc−CB** as an EUV photoresist material, the sample was exposed with an open-frame mask for a dose test known as the contrast curve. The same test was performed on **ZrMc** for comparison. For a contrast curve, multiple spots are exposed to a different EUV dose, and the thickness remaining after the development on each spot indicates the degree of the solubility switch of the resist attained after each dose. In the case of a negative-tone resist, as the ones studied here, a ratio of the layer thickness will remain after the development above a certain dose threshold. This dose threshold is known as the dose-to-gel, D_0, while the dose required to reach the maximum thickness is noted as D_{100}. The contrast factor γ relates both parameters and is defined as $\gamma = 1/\log_{10}(D_{100}/D_0)$. As shown in Figure 1, **ZrMc−CB** is less sensitive to EUV than the nonfunctionalized MOC **ZrMc** as it requires a higher dose to become less soluble in the developer of choice.[31] Table 1 summarizes the D_0, D_{100}, and γ values of both materials with the same developer and development process. The curves did not show a significant improvement or deterioration of the contrast factor but showed a drop of almost 1 order of magnitude in the sensitivity for **ZrMc−CB**. The structural changes after EUV exposure responsible for this effect were investigated via spectroscopic techniques and are detailed in the next section. The top−down SEM image of the line−space

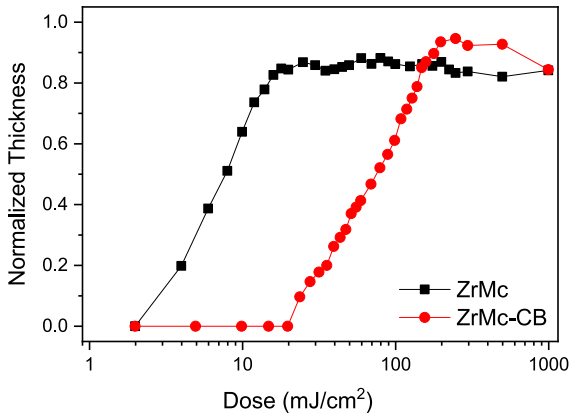

Figure 1. Contrast curves of ZrMc (original thickness: 26.7 nm) and **ZrMc−CB** (original thickness: 29.1 nm), developed in chloroform for 30 s, without the baking treatment.

Table 1. Comparison of the Sensitivity and Contrast Factor between ZrMc and ZrMc−CB[a]

MOC	D_0 (mJ/cm^2)	D_{100} (mJ/cm^2)	γ
ZrMc	2.5 ± 0.3	16.8 ± 1.7	1.2 ± 0.1
ZrMc-CB	22.6 ± 0.8	195.7 ± 7.2	1.1 ± 0.1

[a]Standard deviations were calculated from the error propagation of the slope and intercept of the fitted line between D_0 and D_{100}.

https://doi.org/10.1021/acsami.1c16257
ACS Appl. Mater. Interfaces 2021, 13, 51790−51798

pattern of **ZrMc−CB** (Figure S2) also shows the negative effect of the carbazole unit on the sensitivity of the photoresist: for resolving 50 nm half-pitch patterns, a higher dose (90 mJ/cm^2) was required than that for the **ZrMc** material (57 mJ/cm^2).[22]

Fluorescence Labeling. The incorporation of the CB ligand in **ZrMc** provided **ZrMc−CB** with fluorescence emission, as intended. The fluorescence spectra of the **ZrMc−CB** thin film display an emission band around 430 nm upon UV excitation, while the precursor material **ZrMc** is not fluorescent. We selected three doses to track the changes in the spectral shape after EUV exposure. As shown in Figure 2,

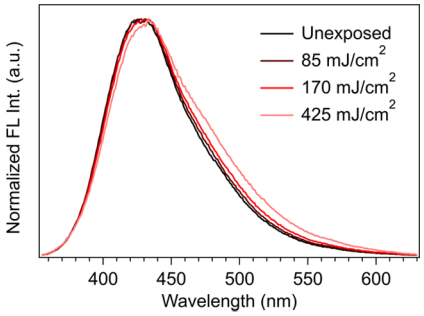

Figure 2. Normalized fluorescence spectra of pristine and EUV-exposed **ZrMc−CB** films on quartz (λ_{exc} = 345 nm).

the emission spectra of exposed samples at doses up to 170 mJ/cm^2 show only the slight broadening of the emission band. At the highest dose of 425 mJ/cm^2, the emission peak red-shifts 6 nm. We conclude that no decarboxylation reaction occurs on the CB ligand as this would yield phenylcarbazole embedded in the film, and its fluorescence should lead to the appearance of a new emission band at *ca.* 378 nm.[32] In general, any bond dissociation that would interrupt the extended aromatic system of the CB ligand would lead to a blue shift of the emission.

The changes in the fluorescence emission intensity of **ZrMc−CB** as a function of the EUV dose were measured with a fluorescence microscope. In the as-exposed sample (no development step applied), fluorescence is reduced with the dose of EUV exposure but still detectable even at the highest applied dose of 994 mJ/cm^2 (Figure 3a). In this sample, the rates of the fluorescence intensity decrease with the dose are different at low- and high-dose regimes, separated at D_{100}. In contrast, in the developed sample, the curve of the fluorescence intensity displays three regimes (Figure 3b). In the first regime, the emission intensity first remains at the background level below D_0; the second regime starts where the intensity increases with the exposure dose up to D_{100}; and above this value, the third regime takes place, in which the sample is overexposed and the emission intensity steadily decreases. Such behavior in the first two regimes is correlated to the remaining thickness of the photoresist after the development at each dose. As shown in the contrast curve (Figure 1), in the exposed areas that received EUV doses below the solubility switch threshold (D_0), no fluorescent material remains on the substrate after immersing the sample into the developer as the material is still soluble in that solvent. The emission intensity increases with the dose between D_0 and D_{100}, in line with the increasing amount of material remaining in that area on the substrate. In fact, when the fluorescence intensity is normalized to the thickness left at the measured spot, a constant value is

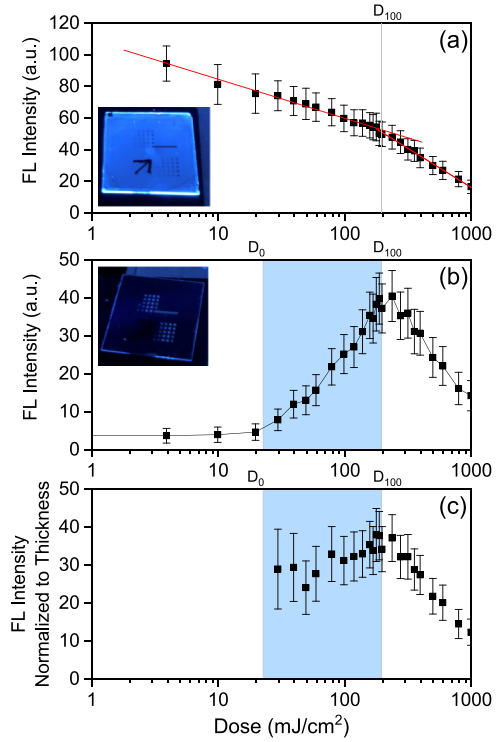

Figure 3. (a) Fluorescence intensity of the **ZrMc−CB** film exposed to the given EUV dose before development. (b) Fluorescence intensity of the **ZrMc−CB** film after development. (c) Fluorescence intensity normalized to the thickness of the developed sample.

obtained for this D_0−D_{100} range (Figure 3c). The third regime displays a decreasing trend in both absolute and normalized scales, in line with the decrease in intensity observed in the undeveloped sample for this dose range.

Therefore, EUV exposure leads to a decrease in the fluorescence emission of **ZrMc−CB** compared to that of the unexposed film. Nevertheless, two different dose ranges were detected; below D_{100}, the insoluble product that keeps forming with the increasing dose emits with a higher intensity than the product that results from overexposure above D_{100}. The origin of the reduced fluorescence can be bleaching or quenching because of the cleavage or modification of the CB ligand and/or the modification of its surroundings upon EUV irradiation so that fluorescence quenching is favored in the environment generated after the exposure.

With fluorescence microscopy, we obtain the fluorescence intensity of each exposed pad as well as the corresponding fluorescence time profiles, thus allowing us to see the evolution of the fluorescence lifetime after EUV exposure before and after the development step (see Figure S5 in the Supporting Information). In the low-dose range up to D_{100}, the average fluorescence lifetime increases from ∼2.4 to 3.2 ns and then stabilizes at this last value. The values are essentially the same for the developed patches and those that were exposed only. We tentatively attribute the increasing lifetime to the rigidification of the matrix resulting from the cross-linking reactions of the Mc ligands, thus enhancing the lifetime of the carbazole residues that we detect. When the film is fully cross-linked (>D_{100}), no further changes in lifetimes are observed.

However, we still observe a gradual decrease in intensity upon exposure, without changes in the shapes of absorption and emission spectra, which implies that the carbazole

https://doi.org/10.1021/acsami.1c16257
ACS Appl. Mater. Interfaces 2021, 13, 51790−51798

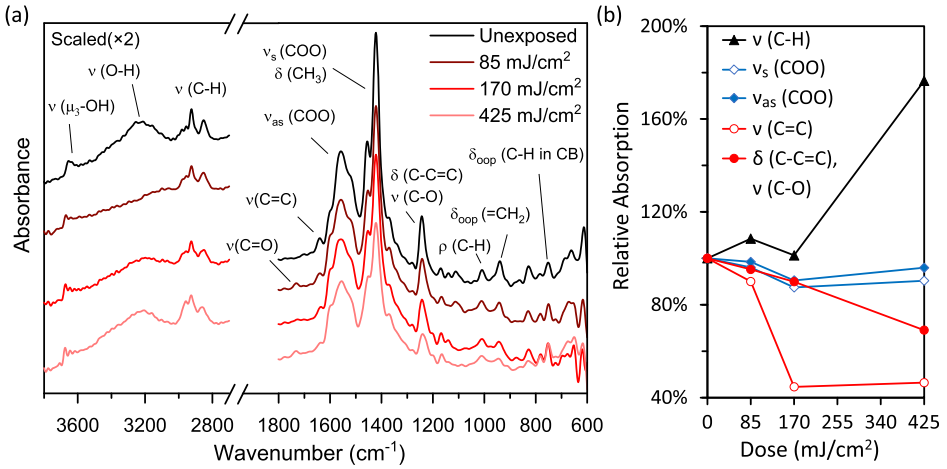

Figure 4. (a) IR absorption spectra of an unexposed **ZrMc−CB** film and films exposed to 85, 170, and 425 mJ/cm^2 of EUV light without development. (b) Change in the relative absorption of C−H, COO, and C═C stretching modes.

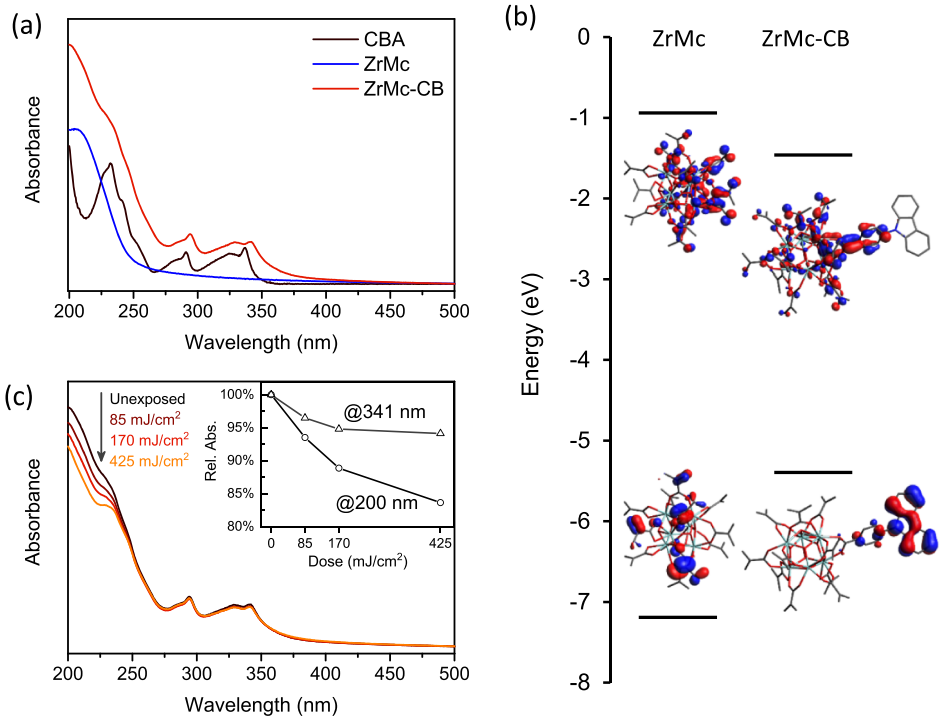

Figure 5. (a) UV absorption spectra of CBA in diluted pentane solution (rescaled ×0.3 for clarity) and ZrMc and **ZrMc−CB** spin-coated thin films on quartz substrates. (b) Frontier orbitals (HOMO and LUMO) of **ZrMc−CB** calculated at the B3LYP level of theory using the Def2SVP basis set. (c) UV absorption spectra of unexposed and EUV-exposed area in the **ZrMc−CB** film. Inset: Absorption spectral changes of **ZrMc−CB** after EUV exposure of different doses normalized to the absorbance of the unexposed sample.

chromophores are not undergoing structural changes. Apparently, a minor fraction of the chromophores is strongly quenched, with lifetimes below the detection limit of our setup. To explain this, we postulate that quenching sites are created near some of the fluorophores, for example, *via* decarboxylation reactions that modify the inorganic core. Further spectroscopic investigations with FTIR and UV−visible absorption spectroscopies were performed to identify the potential paths that would explain the observed behavior in fluorescence microscopy.

Fourier-Transform Infrared Spectra. The FTIR absorption spectra of **ZrMc−CB** films exposed to different EUV doses are shown in Figure 4a, with the spectrum of an unexposed **ZrMc−CB** film as the reference. Because of the low concentration of the carbazole benzoate ligand in the MOC film, the spectrum of **ZrMc−CB** shows features mainly from the Mc ligands.[22,24,33] The bands at 2800−3010 cm^{-1} are ascribed to the C−H stretching of the methyl group, and the absorption at 2960 cm^{-1} shows a significant increase at the dose of 425 mJ/cm^2. The bands in the range of 1350−1450 cm^{-1} are assigned to COO symmetric stretching overlapping with the C−H bending of $-CH_3$, and bands at 1556−1600 cm^{-1} originate from COO asymmetric stretching. The bands centered at 1640 cm^{-1} and 1240 cm^{-1} are due to the C═C stretching mode and C−C═C rocking mode in the Mc, respectively. The relative absorption intensity of these four regions decreases with the EUV irradiation, while the absorption band from the C═C stretching mode bleaches

https://doi.org/10.1021/acsami.1c16257
ACS Appl. Mater. Interfaces 2021, 13, 51790−51798

Scheme 2. (a,b) Hole-Initiated Reactions of the ZrMc−CB Radical Cation Induced by EUV Photons and (c) Intra- or Intermolecular Electron Transfer Competing with (d) TheDecarboxylation of Mc and the Formation of Free Radicals Initiating Cross-Linking

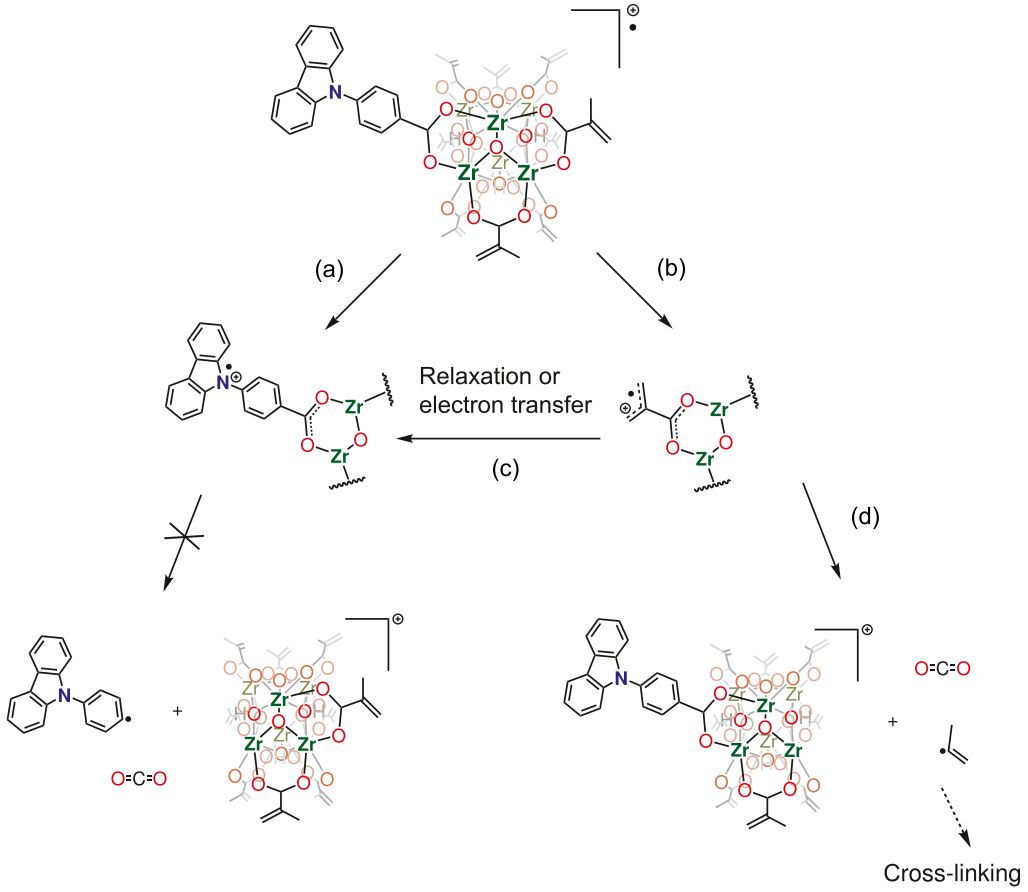

faster than that of COO (Figure 4b). On the other hand, the band centered in 750 cm^{-1} is assigned to the C−H bending mode in the extended aromatic structure in the carbazole benzoate ligand.[34] This absorption band shows no remarkable change after exposure to EUV light. These trends indicate that ligand cleavage and cross-linking reactions happen in the Mc ligands upon EUV irradiation in analogy to the behavior observed for the **ZrMc** precursor.[22]

Unfortunately, the characteristic bands arising from the aromatic ring stretching modes of the CBA unit (in the 1400−1600 cm^{-1} range) cannot be detected in the resist thin film (Figure S6 in the Supporting Information) as this ligand is in a 11:1 ratio to Mc. However, chemical changes in the CBA unit can be tracked by looking at its fingerprints in the UV−vis absorption and emission spectra (see below).

UV−Visible Absorption Spectra. The UV−visible absorption spectra of CBA solution in pentane and **ZrMc** and **ZrMc−CB** thin films are shown in Figure 5a. The spectrum of the **ZrMc−CB** thin film displays a small baseline drift due to light scattering and a slight red shift with respect to that of CBA in solution. In contrast, the UV absorption spectrum of the drop-casted CBA film shows relatively lower intensity for the bands at 291 and 337 nm and a larger red shift compared to that of **ZrMc−CB** (Figure S7 in the Supporting Information). These differences are attributed to the $\pi-\pi$ stacking of the CB units in the solid state, a very common phenomenon in extended aromatic structures and in particular for carbazole derivatives.[35−37] In the UV absorption spectrum of the **ZrMc−CB** thin film, the absorption band around 200 nm is assigned to the $\pi \rightarrow \pi^*$ electronic transition of the Mc ligand. The absorption bands around 230−250, 290, and 330 nm originate from the carbazole unit.[38] The fact that the bands assigned to the CB present almost no shift in **ZrMc−CB** compared to that of CBA in solution indicates that there is no strong electronic interaction between the π-system and the metal−oxo core. This is in agreement with quantum chemistry calculations, which reveal that the introduction of CBA in a Zr MOC brings the highest occupied molecular orbital (HOMO) and lowest unoccupied molecular orbital (LUMO) localized on the CB ligand (Figure 5b). Therefore, the lowest-energy electronic transitions in the **ZrMc−CB** molecule involve mainly the CB unit and are thus promoted at the same wavelengths as in the free CBA ligand.

The inspection of the molecular orbitals can also give relevant hints for the understanding of the mechanisms triggered by radiation. Since EUV photons induce the photoionization of the material, the location of the HOMO indicates where the electron vacancy will be most likely located after the rapid electronic relaxation processes that follow ionization. This information can then help us understand the chemical reactions that the resulting radical cation can undergo (see the subsection below).

After the exposure to EUV light with three different doses, the bleaching of absorption bands was detected (Figure 5c). The absorption band at 200 nm of **ZrMc−CB**, assigned to the $\pi-\pi^*$ electronic transitions located in the Mc ligand, decreased

https://doi.org/10.1021/acsami.1c16257
ACS Appl. Mater. Interfaces 2021, 13, 51790−51798

in line with the bleaching of C=C stretching bands in the FTIR spectra. The carbazole absorption in the 275−370 nm range is only slightly bleached (Figure 5c inset).

Mechanism for the Sensitivity and Fluorescence Intensity Change with CB Ligands. Different from the deep UV exposure, where the absorption and photoexcitation are limited to certain components in resist materials, EUV is mainly absorbed by the atoms with the higher photon absorption cross-sections at 92 eV. In the case of the Zr-based MOC, this is likely to occur at the oxygen atoms. Photoionization of **ZrMc**, in particular, can lead to the formation of allyl radicals, as previously proposed in the literature.[22,39] However, for **ZrMc−CB**, the situation can be more complex. The O atoms of the Mc ligands participate in different molecular orbitals (HOMO-X and below) from that of the O atoms of the CB ligand (from HOMO to HOMO-Y). This means that two different radical cations can be considered, as shown in routes (a) and (b) in Scheme 2. Nevertheless, it is plausible that when a hole is generated in the O of an Mc ligand, the molecule relaxes by the electron decay from the HOMO to the hole at the deeper molecular orbital, thus yielding the radical cation on the CB ligand. It should be mentioned that ionization can also be induced by the generated photoelectrons and secondary electrons when their kinetic energy is higher than the ionization potential of the molecules. In this case, the probability of the ionization on either ligand is not straightforward to predict.

The cross-linking between clusters through Mc ligands is initiated by free radicals.[22,39] Therefore, while Mc ligands can yield free allyl radicals, the radical cation on the carbazole ligands is stabilized and less likely to dissociate. In addition to that, as CB is an electron donor, electron transfer from neutral CB to Mc radical cations can also prevent the formation of allyl radicals. Therefore, as hypothesized in the Introduction section, the reactivity of precursor **ZrMc** is reduced with the incorporation of the carbazole unit to the cluster because of its hole stabilizing property as it decreases the yield of free radicals in the materials upon EUV irradiation.[40] This explains the low reactivity and sensitivity of **ZrMc−CB** in contrast to that of **ZrMc**.

Overall, the spectral changes in the fluorescence, FTIR, and UV absorption spectra of the **ZrMc−CB** films that were exposed to EUV photons up to 170 mJ/cm^2 are in agreement with the promotion of cross-linking and decarboxylation reactions of Mc ligands with EUV exposures previously proposed for the **ZrMc** material. These reactions still seem to play a crucial role for the solubility switch in **ZrMc−CB**, while the carbazole benzoate ligand is rather stable at these doses. At higher doses, 425 mJ/cm^2 for example, the UV absorption band is only bleached by 6% at 341 nm, while the fluorescence emission intensity is about 64% less than that of the unexposed sample. This reveals that the decrease in the fluorescence is not only caused by a lower photon absorption of the excitation light (λ = 345 nm) but also by other quenching mechanisms. It could be argued that some carbazole derivative with a lower fluorescence quantum yield than that of the intact ligand might be formed after EUV exposure. For instance, carbazole radical cations tend to be reactive in positions 3 and 6.[41] If water molecules are present in the film, OH groups could be inserted in position 3 or 6 after the ionization of **ZrMc−CB**, which might affect the fluorescence of the CB unit. However, this kind of modification in the carbazole would also lead to spectral shifts in both the absorption and emission spectra. The subtle spectral changes in the bands associated to CB in UV absorption fluorescence spectra do not support this explanation. Alternatively, the fluorescence quenching could be due to the opening of competing relaxation pathways in the areas that have been chemically modified by EUV light. We hypothesize that decarboxylation reactions occurring in the Mc ligands change the electron affinity of the Zr-based inorganic core. It is plausible that after the partial loss of Mc ligands because of EUV irradiation, the inorganic core acts as an electron acceptor so that the excited states of the carbazole unit relax *via* electron transfer, a path that competes with the emissive relaxation. This might explain the progressive decrease in the fluorescence intensity *versus* dose in Figure 3. At low doses, certain decarboxylation and cross-linking reactions occur. Once the terminal double bonds are depleted (above D_{100}), further decarboxylation events and subsequent processes keep favoring fluorescence quenching.

CONCLUSIONS

In this work, we have demonstrated a straightforward method to functionalize MOCs with a fluorescent label (carbazole benzoate) *via* a ligand exchange reaction. The processability and lithographic contrast of the precursor material are preserved. Nevertheless, the functionalized MOC showed a drop in the sensitivity, which we attribute to the hindering of polymerization reactions, either because the hole is trapped on CB or because the intermolecular packing distance is increased. Fluorescence spectroscopy allowed us to further investigate how the fluorescent label can provide mechanistic information. The carbazole benzoate ligand does not show significant structural changes after EUV exposure. However, its fluorescence is quenched, which we attribute to the changes in the surrounding matrix induced by EUV light. We propose that electron transfer from the excited phenylcarbazole unit to the inorganic cluster is enabled in the exposed areas and therefore competes with the fluorescence emission. From these results, we predict that extended aromatic structures can be utilized in the design of new EUV photoresist materials for tuning the reaction kinetics. Furthermore, we envision that to carry out fluorescent labeling without the deterioration of the resist sensitivity, the ligand exchange can be applied during or after the development for the surface modification of the preexisting nanopatterns.

ASSOCIATED CONTENT

Supporting Information

The Supporting Information is available free of charge at https://pubs.acs.org/doi/10.1021/acsami.1c16257.

NMR spectra; SEM image of line-and-space patterns; sample exposure scheme; atomic force microscopy image of the surface of the spin-coated thin film; fluorescence spectra of samples at different doses; UV absorption spectra of the CBA drop-casted film *versus* solution; fluorescence emission lifetimes as a function of EUV exposure dose; and theoretical calculations (PDF)

AUTHOR INFORMATION

Corresponding Authors

Lianjia Wu − *Advanced Research Center for Nanolithography, Amsterdam 1098XG, The Netherlands;* orcid.org/0000-0002-3061-0059; Email: l.wu@arcnl.nl

https://doi.org/10.1021/acsami.1c16257
ACS Appl. Mater. Interfaces 2021, 13, 51790−51798

Sonia Castellanos − *Advanced Research Center for Nanolithography, Amsterdam 1098XG, The Netherlands;* orcid.org/0000-0002-4880-1910; Email: s.castellanos@arcnl.nl

Authors

Michiel F. Hilbers − *Van 't Hoff Institute for Molecular Sciences, University of Amsterdam, Amsterdam 1090 GD, The Netherlands*

Olivier Lugier − *Advanced Research Center for Nanolithography, Amsterdam 1098XG, The Netherlands*

Neha Thakur − *Advanced Research Center for Nanolithography, Amsterdam 1098XG, The Netherlands;* orcid.org/0000-0001-5252-0938

Michaela Vockenhuber − *Laboratory of Micro and Nanotechnology, Paul Scherrer Institute, Villigen 5232, Switzerland*

Yasin Ekinci − *Laboratory of Micro and Nanotechnology, Paul Scherrer Institute, Villigen 5232, Switzerland*

Albert M. Brouwer − *Advanced Research Center for Nanolithography, Amsterdam 1098XG, The Netherlands; Van 't Hoff Institute for Molecular Sciences, University of Amsterdam, Amsterdam 1090 GD, The Netherlands;* orcid.org/0000-0002-1731-3869

Complete contact information is available at: https://pubs.acs.org/10.1021/acsami.1c16257

Notes

The authors declare no competing financial interest.

■ ACKNOWLEDGMENTS

The authors acknowledge the Paul Scherrer Institute (PSI), Switzerland, for the provision of beamtime at the XIL-II beamline of SLS (proposal 20182117). Part of this work has been carried out within the Advanced Research Center for Nanolithography (ARCNL), a public−private partnership between the University of Amsterdam (UvA), the Vrije Universiteit Amsterdam (VU), the Netherlands Organisation for Scientific Research (NWO), and the semiconductor equipment manufacturer ASML.

■ REFERENCES

(1) Mulkens, J.; Flagello, D. G.; Streefkerk, B.; Gräupner, P. Benefits and Limitations of Immersion Lithography. *J. Micro/Nanolithogr., MEMS, MOEMS* **2004**, *3*, 104−115.

(2) French, R. H.; Tran, H. V. Immersion Lithography: Photomask and Wafer-Level Materials. *Annu. Rev. Mater. Res.* **2009**, *39*, 93−126.

(3) Neisser, M.; Wurm, S. ITRS Lithography Roadmap: Status and Challenges. *Adv. Opt. Technol.* **2012**, *1*, 217−222.

(4) Neisser, M.; Wurm, S. ITRS Lithography Roadmap: 2015 Challenges. *Adv. Opt. Technol.* **2015**, *4*, 235−240.

(5) Levinson, H. J. *Principles of Lithography*; SPIE Press, 2005; Vol. *146*.

(6) Okoroanyanwu, U. *Chemistry and Lithography*; SPIE Press, 2010.

(7) Kozawa, T.; Tagawa, S. Radiation Chemistry in Chemically Amplified Resists. *Jpn. J. Appl. Phys.* **2010**, *49*, 030001−1.

(8) Itani, T.; Kozawa, T. Resist Materials and Processes for Extreme Ultraviolet Lithography. *Jpn. J. Appl. Phys.* **2012**, *52*, 010002.

(9) Cardineau, B.; Del Re, R.; Marnell, M.; Al-Mashat, H.; Vockenhuber, M.; Ekinci, Y.; Sarma, C.; Freedman, D. A.; Brainard, R. L. Photolithographic Properties of Tin-Oxo Clusters Using Extreme Ultraviolet Light (13.5 nm). *Microelectron. Eng.* **2014**, *127*, 44−50.

(10) De Simone, D.; Pollentier, I.; Vandenberghe, G. Metal-Containing Materials as Turning Point of EUV Lithography. *J. Photopolym. Sci. Technol.* **2015**, *28*, 507−514.

(11) Xu, H.; Sakai, K.; Kasahara, K.; Kosma, V.; Yang, K.; Herbol, H. C.; Odent, J.; Clancy, P.; Giannelis, E. P.; Ober, C. K. Metal−Organic Framework-Inspired Metal-Containing Clusters for High-Resolution Patterning. *Chem. Mater.* **2018**, *30*, 4124−4133.

(12) Kreutzer, J.; Puchberger, M.; Artner, C.; Schubert, U. Retention of the Cluster Core Structure during Ligand Exchange Reactions of Carboxylato-Substituted Metal Oxo Clusters. *Eur. J. Inorg. Chem.* **2015**, *2015*, 2145−2151.

(13) Walther, P.; Puchberger, M.; Kogler, F. R.; Schwarz, K.; Schubert, U. Ligand Dynamics on the Surface of Zirconium Oxo Clusters. *Phys. Chem. Chem. Phys.* **2009**, *11*, 3640−3647.

(14) Kolodner, P.; Katzir, A.; Hartsough, N. End-Point Detection and Etch-Rate Measurement during Reactive-Ion Etching Using Fluorescent Polymer Films. *J. Vac. Sci. Technol. B* **1983**, *1*, 501−504.

(15) Kimura, S.; Takami, K. Photoresist Thickness Measurement Using Laser-Induced Fluorescence. *Appl. Opt.* **1988**, *27*, 3675−3678.

(16) Mizokuro, T.; Mochizuki, H.; Tanigaki, N.; Mo, X.; Yamamoto, N.; Hiraga, T. Fabrication of Fluorescence Micropatterns to Photoresists by Selective Doping of Fluorescent Dye Using Vapor Transportation Method. *Jpn. J. Appl. Phys.* **2005**, *44*, L1449−L1451.

(17) Ciardelli, F.; Ruggeri, G.; Pucci, A. Dye-Containing Polymers: Methods for Preparation of Mechanochromic Materials. *Chem. Soc. Rev.* **2013**, *42*, 857−870.

(18) Sundararajan, P. R. Small Molecule Self-Assembly in Polymer Matrices. *J. Polym. Sci., Part B: Polym. Phys.* **2018**, *56*, 451−478.

(19) Berro, A. J.; Berglund, A. J.; Carmichael, P. T.; Kim, J. S.; Liddle, J. A. Super-Resolution Optical Measurement of Nanoscale Photoacid Distribution in Lithographic Materials. *ACS Nano* **2012**, *6*, 9496−9502.

(20) Messinis, C.; Tenner, V. T.; De Boer, J. F.; Witte, S.; den Boef, A. Impact of Coherence Length on the Field of View in Dark-Field Holographic Microscopy for Semiconductor Metrology: Theoretical and Experimental Comparisons. *Appl. Opt.* **2020**, *59*, 3498−3507.

(21) Wu, L.; Tiekink, M.; Giuliani, A.; Nahon, L.; Castellanos, S. Tuning Photoionization Mechanisms of Molecular Hybrid Materials for EUV Lithography Applications. *J. Mater. Chem. C* **2019**, *7*, 33−37.

(22) Wu, L.; Baljozovic, M.; Portale, G.; Kazazis, D.; Vockenhuber, M.; Jung, T.; Ekinci, Y.; Castellanos, S. Mechanistic Insights in Zr-and Hf-Based Molecular Hybrid EUV Photoresists. *J. Micro/Nanolithogr., MEMS, MOEMS* **2019**, *18*, 013504.

(23) Del Re, R.; Passarelli, J.; Sortland, M.; Cardineau, B.; Ekinci, Y.; Buitrago, E.; Neisser, M.; Freedman, D. A.; Brainard, R. L. Low-Line Edge Roughness Extreme Ultraviolet Photoresists of Organotin Carboxylates. *J. Micro/Nanolithogr., MEMS, MOEMS* **2015**, *14*, 043506.

(24) Mattson, E. C.; Cabrera, Y.; Rupich, S. M.; Wang, Y.; Oyekan, K. A.; Mustard, T. J.; Halls, M. D.; Bechtel, H. A.; Martin, M. C.; Chabal, Y. J. Chemical Modification Mechanisms in Hybrid Hafnium Oxo-Methacrylate Nanocluster Photoresists for Extreme Ultraviolet Patterning. *Chem. Mater.* **2018**, *30*, 6192−6206.

(25) Kickelbick, G.; Schubert, U. Oxozirconium Methacrylate Clusters: $Zr_6(OH)_4O_4(OMc)_{12}$ and $Zr_4O_2(OMc)_{12}$ (OMc = Methacrylate). *Chem. Ber.* **1997**, *130*, 473−478.

(26) Liou, G.-S.; Hsiao, S.-H.; Huang, N.-K.; Yang, Y.-L. Synthesis, Photophysical, and Electrochromic Characterization of Wholly Aromatic Polyamide Blue-Light-Emitting Materials. *Macromolecules* **2006**, *39*, 5337−5346.

(27) Hsiao, S.-H.; Chiu, Y.-T. Electrosynthesis and Electrochromic Properties of Poly(amide-triarylamine)s Containing Triptycene Units. *RSC Adv.* **2015**, *5*, 90941−90951.

(28) Frisch, M. J.; Trucks, G. W.; Schlegel, H. B.; Scuseria, G. E.; Robb, M. A.; Cheeseman, J. R.; Scalmani, G.; Barone, V.; Petersson, G. A.; Nakatsuji, H.; Li, X.; Caricato, M.; Marenich, A.; Bloino, J.; Janesko, B. G.; Gomperts, R.; Mennucci, B.; Hratchian, H. P.; Ortiz, J. V.; Izmaylov, A. F.; Sonnenberg, J. L.; Williams-Young, D.; Ding, F.; Lipparini, F.; Egidi, F.; Goings, J.; Peng, B.; Petrone, A.; Henderson,

T.; Ranasinghe, D.; Zakrzewski, V. G.; Gao, J.; Rega, N.; Zheng, G.; Liang, W.; Hada, M.; Ehara, M.; Toyota, K.; Fukuda, R.; Hasegawa, J.; Ishida, M.; Nakajima, T.; Honda, Y.; Kitao, O.; Nakai, H.; Vreven, T.; Throssell, K.; Montgomery, J. A.; Peralta, J.; Ogliaro, F.; Bearpark, M.; Heyd, J. J.; Brothers, E.; Kudin, K. N.; Staroverov, V. N.; Keith, T.; Kobayashi, R.; Normand, J.; Raghavachari, K.; Rendell, A.; Burant, J. C.; Iyengar, S. S.; Tomasi, J.; Cossi, M.; Millam, J. M.; Klene, M.; Adamo, C.; Cammi, R.; Ochterski, J. W.; Martin, R. L.; Morokuma, K.; Farkas, O.; Foresman, J. B.; Fox, D. J. *Gaussian 16*, Revision A.03; Gaussian, Inc.: Wallingford CT, 2016.

(29) Andrae, D.; Häußermann, U.; Dolg, M.; Stoll, H.; Preuß, H. Energy-Adjusted ab initio Pseudopotentials for the Second and Third Row Transition Elements. *Theor. Chim. Acta* **1990**, *77*, 123−141.

(30) Weigend, F.; Ahlrichs, R. Balanced Basis Sets of Split Valence, Triple Zeta Valence and Quadruple Zeta Valence Quality for H to Rn: Design and Assessment of Accuracy. *Phys. Chem. Chem. Phys.* **2005**, *7*, 3297−3305.

(31) Campbell, S. A. *The Science and Engineering of Microelectronic Fabrication*; Oxford University Press, 1996.

(32) Tang, G.-M.; Chi, R.-H.; Wan, W.-Z.; Chen, Z.-Q.; Yan, T.-X.; Dong, Y.-P.; Wang, Y.-T.; Cui, Y.-Z. Tunable Photoluminescent Materials Based on Two Phenylcarbazole-Based Dimers through the Substituent Groups. *J. Lumin.* **2017**, *185*, 1−9.

(33) Kreutzer, J.; Blaha, P.; Schubert, U. Assessment of Different Basis Sets and DFT Functionals for the Calculation of Structural Parameters, Vibrational Modes and Ligand Binding Energies of Zr_4O_2(carboxylate)$_{12}$ Clusters. *Comput. Theor. Chem.* **2016**, *1084*, 162−168.

(34) Lao, W.; Xu, C.; Ji, S.; You, J.; Ou, Q. Electronic and Vibrational Spectra of a Series of Substituted Carbazole Derivatives. *Spectrochim. Acta, Part A* **2000**, *56*, 2049−2060.

(35) Ding, Z.; Zhao, Q.; Xing, R.; Wang, X.; Ding, J.; Wang, L.; Han, Y. Detection of Explosives with Porous Xerogel Film from Conjugated Carbazole-Based Dendrimers. *J. Mater. Chem. C* **2013**, *1*, 786−792.

(36) Liu, S.; Lin, P.; Niu, F.; Zeng, P.; Zhang, B. π-Bridge Effect on Symmetric Carbazole-Based Small Molecules for Realizing Ultraviolet Fluorescent Emission. *Materials* **2018**, *11*, 617.

(37) Hu, L.; Liu, S.; Xie, G.; Yang, W.; Zhang, B. Bis-(benzothiophene-S, S-dioxide) Fused Small Molecules Realize Solution-Processible, High-Performance and Non-Doped Blue Organic Light-Emitting Diodes. *J. Mater. Chem. C* **2020**, *8*, 1002−1009.

(38) Bonesi, S. M.; Erra-Balsells, R. Electronic Spectroscopy of Carbazole and N- and C-Substituted Carbazoles in Homogeneous Media and in Solid Matrix. *J. Lumin.* **2001**, *93*, 51−74.

(39) Passarelli, J.; Murphy, M.; Del Re, R.; Sortland, M.; Dousharm, L.; Vockenhuber, M.; Ekinci, Y.; Neisser, M.; Freedman, D. A.; Brainard, R. L. High-Sensitivity Molecular Organometallic Resist for EUV (MORE). *Proc. SPIE* **2015**, *9425*, 94250T.

(40) Chapiro, A. Radiation Induced Polymerization. *Radiat. Phys. Chem.* **1979**, *14*, 101−116.

(41) Ambrose, J. F.; Carpenter, L. L.; Nelson, R. F. Electrochemical and Spectroscopic Properties of Cation Radicals: III. Reaction Pathways of Carbazolium Radical Ions. *J. Electrochem. Soc.* **1975**, *122*, 876.

https://doi.org/10.1021/acsami.1c16257
ACS Appl. Mater. Interfaces 2021, 13, 51790−51798